Paper:
Wilson, P. & Matthews, J. (2016). Age assessment and implications of late Quaternary periglacial and paraglacial landforms on Muckish Mountain, northwest Ireland, based on Schmidt-hammer exposure-age dating (SHD). *Geomorphology, 270*, 134-144.
http://dx.doi.org/10.1016/j.geomorph.2016.07.002

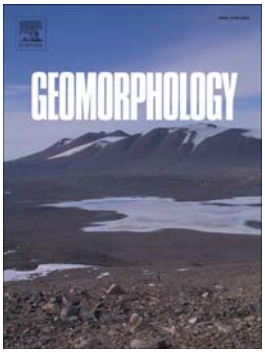

Age assessment and implications of late Quaternary periglacial and paraglacial landforms on Muckish Mountain, northwest Ireland, based on Schmidt-hammer exposure-age dating (SHD)

Peter Wilson, John A. Matthews

PII: S0169-555X(16)30193-3
DOI: doi: 10.1016/j.geomorph.2016.07.002
Reference: GEOMOR 5674

To appear in: *Geomorphology*

Received date: 13 April 2016
Revised date: 14 June 2016
Accepted date: 2 July 2016

Please cite this article as: Wilson, Peter, Matthews, John A., Age assessment and implications of late Quaternary periglacial and paraglacial landforms on Muckish Mountain, northwest Ireland, based on Schmidt-hammer exposure-age dating (SHD), *Geomorphology* (2016), doi: 10.1016/j.geomorph.2016.07.002

Age assessment and implications of late Quaternary periglacial and paraglacial landforms on Muckish Mountain, northwest Ireland, based on Schmidt-hammer exposure-age dating (SHD)

Peter Wilson[a*] and John A. Matthews[b]

[a]*Environmental Sciences Research Institute, School of Geography and Environmental Sciences, Ulster University, Cromore Road, Coleraine, Co. Londonderry BT52 1SA, Northern Ireland, UK*

[b]*Department of Geography, College of Science, Swansea University, Singleton Park, Swansea SA2 8PP, Wales, UK*

**Corresponding author*
E-mail addresses: P.Wilson@Ulster.ac.uk (P. Wilson), J.A.Matthews@Swansea.ac.uk (J.A. Matthews)

Abstract

Schmidt-hammer exposure-age dating (SHD) was applied to a variety of late Quaternary periglacial and paraglacial landforms composed of coarse rock debris on Muckish Mountain, northwest Ireland. Landform ages were determined using a linear high-precision age-calibration curve, derived from young and old control surfaces of known age on the same rock type. The SHD ages represent *maximum* estimates of the time elapsed since the boulders stabilised and the landforms became inactive. Most ages are also *minimum* estimates for the start of landform development because older boulders are buried beneath the sampled surface boulders. Ages and 95% confidence intervals obtained for blockfield, boulder lobes and talus indicate these features were likely active during several of the early Holocene cold events evidenced in Greenland ice cores and North Atlantic sediment records. Activity ceased at different times ~9-7 ka BP. These landforms are the first indication of a geomorphological response to early Holocene cooling in the oceanic mountains of Ireland. Late Holocene ages, obtained for rock-slope failure run-out debris and debris cone boulders, overlap with shifts to cooler and/or wetter conditions, including the Little Ice Age. Geomorphological impacts associated with these changes in climate have not previously been recorded in the Irish uplands. The SHD results indicate that previously implied timings for the stabilisation of some accumulations of coarse rock debris on mountain slopes are in need of revision.

Keywords:

Schmidt-hammer exposure-age dating (SHD)
Periglacial and paraglacial landforms
Holocene climate variability
Maritime periglacial environment
Northwest Ireland

1. Introduction

Establishing the age of late Quaternary landforms is a critical aspect of landscape studies. By placing landforms on a secure chronological footing the timing of geomorphic processes can be constrained. In turn, this assists our understanding of the link between landform development and changes of climate. Of the wide range of techniques currently available for determination of landform age, radiocarbon dating (^{14}C), optically stimulated luminescence (OSL) dating, and terrestrial cosmogenic nuclide surface exposure dating (TCND) are routinely used because of their broad temporal ranges; each method being applicable to a specific type of material. However, these techniques are costly, especially so because multiple, rather than single, samples normally require analysis in order to obtain a reliable estimate of landform or event age. In contrast, Schmidt-hammer exposure-age dating (SHD) has been developed as a high-precision method of absolute or calibrated-age dating and has several advantages over the techniques listed above namely: (1) it is a relatively inexpensive procedure; (2) it does not require laboratory facilities; and (3) it can generate large amounts of data based on the large sample sizes necessary for precise calibration equations and age estimates, within a short period of fieldwork. Furthermore, SHD ages have been shown to be largely consistent with ages derived from TCND (Winkler, 2009; Matthews and Winkler, 2011; Linge et al., in preparation).

Initial applications of the Schmidt-hammer in geomorphology focussed on its ability to distinguish the relative age of landforms by relating the compressive strength of bedrock or boulders to the degree of surface weathering and therefore the surface exposure age (Matthews and Shakesby, 1984; Ballantyne, 1986; McCarroll, 1989). Some later studies have followed this approach (Clark and Wilson, 2004; Frauenfelder et al., 2005; Winkler, 2005) while others have developed the technique into one of high-precision calibrated-age dating (Matthews and Owen, 2010; Shakesby et al., 2011; Matthews and Wilson, 2015; Matthews et al., 2015). Irrespective of the strategy adopted, the Schmidt-hammer has been used for landform age estimation in a wide variety of geomorphic contexts, for example: fluvial terraces (Stahl et al., 2013), flood sediments (McEwan and Matthews, 2013; Matthews

and McEwan, 2013), alluvial fans (White et al., 1998; McEwan et al., in prep), debris flows (Boelhouwers et al., 1999), glacial landforms (Evans et al., 1999; Aa and Sjåstad, 2000; Winkler, 2005, 2009, 2014; Shakesby et al., 2006; Matthews and Owen, 2010; Matthews and Winkler, 2011; Kłapyta, 2013; Ffoulkes and Harrison, 2014; Matthews et al., 2014; Tomkins et al., 2016), active and relict rock glaciers (Aoyama, 2005; Frauenfelder et al., 2005; Kellerer-Pirklbauer et al., 2008; Rode & Kellerer-Pirklbauer, 2012; Matthews et al., 2013), pronival ramparts (Matthews et al., 2011; Matthews and Wilson, 2015), patterned ground (Cook-Talbot, 1991; Winkler et al., 2016), blockstreams (Wilson et al., 2016), snow-avalanche impact ramparts (Matthews et al., 2015), rock-slope failures (Nesje et al., 1994; Clark and Wilson, 2004; Aa et al., 2007; Wilson 2007, 2009a; Owen et al., 2010), chemically-weathered bedrock surfaces (Owen et al., 2007), raised boulder-dominated shorelines (Sjöberg, 1990; Sjöberg and Broadbent, 1991; Shakesby et al., 2011), and shore platforms (Stephenson and Kirk, 2000; Knight and Burningham, 2011).

High-precision absolute SHD requires establishment of a reliable calibration equation derived from at least two control surfaces of known age and of the same rock type as the landforms to be dated (Matthews and Owen, 2010; Matthews and Winkler 2011; Matthews and Wilson, 2015). The method enables construction of 95% confidence intervals around the control surface ages and determination of SHD ages for the landforms under investigation.

This approach has been applied to an assemblage of late Quaternary periglacial and paraglacial landforms composed of coarse rock debris on Muckish Mountain, northwest Ireland. Previous studies in which high-precision absolute SHD was utilised have focussed on single-category landforms such as moraines (Matthews et al., 2014), pronival ramparts (Matthews and Wilson, 2015) and flood berms (Matthews and McEwan, 2013). In this paper we use SHD to assess the age of boulders incorporated into blockfield, boulder lobes, talus, rock-slope failure (RSF) run-out debris, and debris cone on a single rock type on an individual mountain in an oceanic/maritime periglacial environment. Given that different processes are involved in the production of these landforms the aims of the research were: (1) to determine when the debris accumulations and formative processes were last active, (2)

to consider landform ages in relation to patterns of climate change, and (3) to evaluate the precision of the method relative to TCND ages from the same rock type in the same area and therefore to contribute to assessments of the utility of SHD as a calibrated age-dating technique.

2. Research location

Muckish (Lat. 55°06' N, Long 8°00' W; 666 m above sea level (asl); Fig. 1) is part of a 30 km-long southwest-to-northeast aligned tract of the Lower Dalradian Ards quartzite in County Donegal, northwest Ireland. It is steep on all sides except the west and has an extensive plateau above ~600 m asl. Ice from the granite-dominated mountains to the south was thought by Charlesworth (1924) to have crossed the summit of Muckish during the last (Midlandian) glaciation but granite erratics have not been reported from the plateau. Charlesworth also considered the angular quartzite debris on the plateau to be a product of frost activity following withdrawal of glacier ice. Ballantyne et al. (2007) figured Muckish as one of several Donegal mountain tops that escaped glacial erosion during the Last Glacial Maximum (LGM) because ice-scoured bedrock was not seen above ~470 m asl, and the upper limit of erratics on neighbouring mountains is ~550 m asl (Wilson, 1993). Based on evidence demonstrating that the last British-Irish Ice Sheet extended to the Atlantic shelf edge, ~90 km west of the Donegal coastline (O'Cofaigh et al., 2012), Ballantyne et al. (2013) proposed that during the LGM the summit of Muckish was likely covered by cold-based ice frozen to the underlying substrate.

The mean annual temperature on the summit of Muckish, inferred from data at a site close to sea level using a lapse rate of 1 ºC / 100 m (Rohan, 1986), is 4.9 ºC and the mean annual minimum air temperature is 1.4 ºC. Mean monthly minimum values may be below 0 ºC for six months of the year (November-April inclusive). Monthly precipitation figures are not available but small-scale maps place Muckish within the 2000 mm annual isohyet (Rohan, 1986). These data indicate a maritime periglacial regime at the southern limit of the subpolar oceanic zone (Wilson and Sellier, 1995).

3. Debris Landforms

Notwithstanding the issue of ice cover during the LGM, Muckish has several areas occupied by periglacial and paraglacial landforms composed of coarse rock debris about which there is negligible chronological information. These include blockfield, relict and active patterned ground, boulder lobes, debris cone, RSF run-out debris, and talus (Fig. 1), several of which indicate a formerly severe periglacial climatic regime with associated permafrost.

A large arcuate debris ridge of 2.8 M m^3 at the foot of the southwest-facing talus was interpreted by Wilson (1990a) as a relict rock glacier (Figs 1 and 2a). This view has since been amended and the ridge is now considered a consequence of rock-slope failure (Wilson, 2004). TCND (^{10}Be ages) of surface boulders on the ridge (Fig. 2b) yielded weighted mean ages of 16 ka and 15 ka, depending on the production rate used for age calculation (Ballantyne et al., 2013). Boulders within and on the surface of this feature were used as young and old control surfaces (see below).

The summit plateau is dominated by boulders; the largest clasts are concentrated in a zone around the highest point at the northeast extremity (Figs 1 and 2c). Many of the boulders have a *b* axis exceeding 50 cm. Further west and south, boulder sizes decrease markedly and relict patterned ground with superimposed active forms is extensive (Wilson and Sellier, 1995).

Boulder lobes occupy the west-facing slopes of Muckish between 600-550 m asl and 500-350 m asl (Figs 1 and 2d). Some lobes have merged laterally to create terraces with recessed frontal margins. Boulder *b* axes are generally within the range 30-50 cm and lobe/terrace fronts rise up to 5 m above the base of their frontal slopes.

The southwest slopes below 500 m asl are diversified by a broad (450 m wide) rectilinear talus sheet below degraded cliffs (Wilson, 1990b), broad mounds of RSF run-out debris originating from a westward continuation of the same cliff-line, and a debris cone that issues from a deeply incised upland valley (Figs 1, 2e-h). The cone is one of the largest such features in the mountains of Ireland; it is 530 m in length, extends through a height range of

180 m and has a basal width of 200 m. The lower part of the cone stands at gradients of up to 33° for 30-40 m above which the general surface slope to the apex, at the mouth of the upland valley, is in the range ~15-20° (Sellier and Wilson, 1995).

4. Methods and rationale

Schmidt-hammer R-values were obtained from surface boulders on the different landforms using a mechanical 'N-type' Schmidt hammer (Proceq, 2006), the reliability of which was checked before and after use with the manufacturer's test anvil (McCarroll, 1987, 1994; Winkler and Matthews, 2014). Mean R-values were derived from two impacts on each of 150 boulders at each control site and at eight locations on the landforms selected for investigation (Fig. 1). Boulder surfaces selected for SHD measurements were horizontal or near-horizontal, and corners, cracks, and lichen thalli were avoided (Matthews and Wilson, 2015); data collection was done in dry conditions and by a single operator.

The young control site comprised boulders exposed by quarrying of the large RSF debris ridge at the foot of the southwest-facing slopes (Figs 1 and 2a). A quarry has existed here for at least 35 years but was substantially extended and deepened about 25 years ago and has since been worked intermittently. The sampled boulders came from locations excavated within the last 25 years and ~10-15 m below the ridge crest. An age of 20 years was assigned to this control site. Boulders on the surface of the debris ridge near to its eastern end were used as the old control site (Figs 1, 2a). Based on the ^{10}Be weighted mean ages of 16 ka and 15 ka from boulders on this part of the ridge (Fig. 2b) an age of 15.5 ka was assigned to the site.

The landforms sampled for SHD are those described in section 3 (above) and as indicated on Fig. 1 and shown in Figs 2c-h. Single sites were selected for sampling on summit blockfield and talus accumulation; two sites were sampled at different elevations on each of the other landforms.

The high-precision calibration equation was based on data for both the young and old control surfaces (Table 1). The equations used to derive the age calibration equation,

including the calculation of 95% confidence intervals around predicted SHD ages, are as outlined by Matthews *et al*. (2014) and Matthews and Wilson (2015). The calibration equation is a standard linear regression equation of the form:

$$y = a + bx$$

where x is mean R-value and y is surface age in years. For two control points, the b coefficient (slope of the calibration curve) is defined by:

$$b = (y_1 - y_2)/(x_1 - x_2)$$

where x_1 and x_2 are the mean R-values of the older and younger control points, respectively, and y_1 and y_2 are their respective ages. The a coefficient (intercept age) is obtained by substitution in the calibration equation.

The 95% confidence interval for age, which represents the total error (C_t), combines the error of the calibration curve at the point associated with the sample surface being dated (C_c) with the sampling error residing in the sample itself (C_s):

$$C_t = \sqrt{(C_c^2 + C_s^2)}$$

The error of the calibration curve is calculated from the errors associated with the control points and their difference in age:

$$C_c = C_o - [(C_o - C_y)(R_s - R_o)/(R_y - R_o)]$$

where C_o is the 95% confidence interval of the old control point in years, C_y is the confidence interval of the young control point in years, and R_o, R_y and R_s are the mean R-values of the old control point, the young control point and the sample surface, respectively. The sampling

error associated with the sample surface depends on the slope of the calibration curve (*b*), the sample size (*n*), Student's *t* statistic and the standard deviation (*s*) of the R-values from the sample surface:

$C_s = b[ts/\sqrt{(n-1)}]$

As with previous high-precision calibrated SHD studies in which two control surface of known age were used (Matthews and Owen, 2010; Matthews and Winkler 2011; Matthews and Wilson, 2015; Matthews et al., 2015) we have inferred a linear R-value–age relationship between the young and old control sites on Muckish. These earlier investigations were restricted to the Holocene timescale (<11.7 ka) and the adoption of a linear relationship is justified because: (1) weathering rates of hard crystalline rocks are slow and, in principle, near-linear on the Holocene timescale (e.g. Colman, 1981; Colman and Dethier, 1986); and (2) tests using several intermediate and firmly dated age-control points on granite surfaces (Shakesby et al., 2011) have demonstrated a linear trend on the Holocene timescale.

As our old control point is ~4 ka prior to the start of the Holocene use of a linear relationship may be questioned. However, a linear calibrated-age curve extending to ~15 ka has been suggested by Engel (2007) for granite surfaces in the Czech Republic, and Sánchez et al. (2009) indicated that R-values continue to decline in a linear manner on granite surfaces up to ~70 ka in northwest Spain. Furthermore, field data demonstrating low rates of post-glacial weathering for hard crystalline rocks rich in quartz/quartzite are available for arctic-alpine areas of Scandinavia (Andre, 1996, 2002; Nicholson, 2008). Similar rates had been previously recorded in cool temperate areas of Canada (Clément et al., 1967) and southern Sweden (Rundberg, 1970) suggesting that the weathering of such rocks proceeds at comparable rates in both mid- and high latitude environments. In addition, Tomkins et al. (2016) illustrate a linear trend for the weathering of granite surfaces over the post-LGM - Lateglacial timescale (~23-12 ka) in Great Britain. Given the relatively brief time that has elapsed since withdrawal of LGM ice from Ireland and considering the associated switching

between arctic and cool temperate climate states within this period, we consider use of a linear R-value–age relationship for the Muckish quartzite control sites to be appropriate.

5. Results

5.1 Control sites and the calibration curve

Schmidt hammer R-values for the young and old control sites are summarised in Table 1 and frequency distributions are shown in Fig. 3. These data indicate an R-value difference of 20.4 between boulders recently exposed by quarrying operations from deep within the RSF debris ridge (~20 years; mean R-value 65.6) and the boulders on the surface of the ridge (~15.5 ka; mean R-value 45.2). The range of values for the young site (28) is smaller than for the old control site (48) indicating relatively clustered and dispersed frequency distributions respectively. Furthermore, while the near-symmetrical frequency distribution for the old control site is interpreted as reflecting a single population of boulders, the young control site is slightly negatively skewed suggesting the possibility that a small sub-population of boulders that are more weathered and therefore older than the majority. These boulders may have resided near to or on the surface of the debris ridge prior to quarrying and have been brought to their present location by that activity. The high-precision calibration curve and equation of y = 49798.824 - 758.82353x shown in Fig. 4 was derived from these data.

5.2 Debris landforms and the SHD ages

Schmidt hammer R-values for the debris landforms selected for study are given in Table 2 and frequency distributions are presented in Fig. 5. The blockfield, boulder lobe and talus samples have mean R-values in the range 52.1 to 54.2. These values are numerically closer to the mean R-value of the old control site than the young site. In contrast, the RSF run-out debris and debris cone have mean R-values in the range 63.2 to 65.3 and are numerically closer to the mean R-value of the young control site than the old site. This is mirrored by the shape of the respective frequency distributions. All the distributions display a

degree of negative skewness, and this is more prominent for the blockfield, talus and boulder lobe samples. A mixed population of boulders is therefore indicated with a small but substantial proportion of boulders being more weathered and hence older than the majority. Negative skewness is less pronounced for the RSF run-out debris and debris cone samples suggesting that older boulders have made only minor contributions to these datasets. The implications of these admixtures are considered below.

The SHD exposure ages for the debris landforms, based on their mean R-values, were determined from the calibration equation in Fig. 4. These ages and their 95% confidence intervals (C_t), together with the error components used to determine the confidence intervals – i.e. the sampling error associated with each landform sample (C_s) and the error in the calibration curve (C_c) – are listed in Table 3. Landform ages range from 10.3±1.3 ka to 0.25±0.93 ka and two distinct age clusters are apparent. Cluster 1 comprising blockfield, boulder lobes and talus is early Holocene in age (10.3±1.3 - 8.7±1.6 ka), and cluster 2, late Holocene in age (1.8±1.0 - 0.25±0.9 ka), comprises the RSF run-out debris and the debris cone. Within each age cluster the 95% confidence intervals of the landform ages overlap, so the ages cannot be regarded as statistically different from one another at the 5% significance level.

6. Discussion

Each of the SHD age determinations represents an estimate of the average age of boulders at the surface of their respective landforms. With one exception (i.e. the debris cone upper site) the landforms show no evidence of current activity and assuming there has not been any post-depositional disturbance, the SHD ages are *maximum* estimates of the time elapsed since the boulders stabilised and the landforms became inactive. For several landforms older boulders are buried beneath the sampled surface boulders, in these cases the SHD ages can also be considered as *minimum* estimates for the start of landform development.

6.1 Implications of the early Holocene SHD ages

It is inferred that the blockfield and boulder lobes were active as the upper slopes of Muckish emerged from beneath ice of the last glaciation ~19-16 ka (Clark et al., 2009; Ballantyne et al., 2013). However, the blockfield is likely to be older, having survived under cold-based ice of the LGM, as demonstrated for mountain-top blockfields elsewhere in Ireland (Ballantyne and Stone, 2015), Scotland (Fabel et al., 2012) and Norway (Fjellanger et al., 2006; Juliussen and Humlum, 2007; Goehring et al., 2008). Irrespective of when the Muckish blockfield first developed it is likely to have been active following ice withdrawal because a severe periglacial (permafrost) climate prevailed (Wilson, in press). Also, a periglacial climate on Muckish during part of the Lateglacial Interstadial (14.7-12.9 ka BP) cannot be excluded, and the Younger Dryas Stadial (12.9-11.7 ka BP) was again characterised by permafrost (Wilson, in press).

Stabilisation of the blockfield and boulder lobes occurred in the early Holocene (Table 3). The SHD 95% confidence limits determined for these landforms overlap with two or more of the five short intervals of climatic deterioration (cooling) at around 11.4, 10.9, 10.2, 9.3 and 8.2 ka BP (Figure 6) that are evidenced by ice-rafted debris in North Atlantic sediment cores and/or the $\delta^{18}O$ record of the NGRIP ice core (Bond et al., 1997; Vinther et al., 2006). This suggests that the coarse debris accumulations may have been intermittently active throughout the early Holocene. Although the geomorphological impact of early Holocene cold events in the uplands of Ireland is not yet known, evidence from elsewhere in northwestern Europe indicates that sea surface temperature and mean annual air temperature fell by >2 °C during the 9.3 and 8.2 ka BP events (Klitgaard-Kristensen et al., 1998; Marshall et al., 2007) and this is likely to have been the driver of landscape change. For example, enhanced soil erosion coincident with the 8.2 ka BP event has been documented in Sweden (Zillén and Snowball, 2009; Snowball et al., 2010), Denmark (Hede et al., 2010), and northwest England (Vincent et al., 2011); woodland perturbation and an increase in the representation of cold tolerant trees such as *Betula* and *Pinus* at the expense of thermophilous taxa *Corylus* and *Quercus* have been recorded during the same event in Ireland (Ghilardi and O'Connell,

2013; Holmes et al., 2016) and Denmark (Hede et al., 2010); and from western Scotland pollen evidence indicates the expansion of grassland, and the analysis of ^{14}C dated 'activity events' suggested a dramatic collapse in the Mesolithic population, both at 8.2 ka BP (Wicks and Mithen, 2014). Given these diverse correlations with the 8.2 ka BP event it is not unreasonable to infer that earlier cold phases also had significant landscape impacts, including on high ground in Ireland. Our SHD ages for the blockfield and boulder lobes suggest reactivation of the mountain-top detritus was a likely consequence of these short-lived cold excursions and represent the first indication from the Irish uplands of a geomorphological response to early Holocene cooling events. Reactivation of these features explains their negatively-skewed R-value frequency distributions (Fig. 5). Some older, more weathered boulders appear to have been 'recycled' as a result of renewed cooling, with frost heave, boulder overturning and downslope movement accounting for the range of R-values.

Some support for a causal link between early Holocene cold events and activity of the debris accumulations may be provided by the SHD age and 95% confidence limits for the talus (Table 3; Fig. 6). The confidence limits overlap with the most recent of the cold events at 9.3 and 8.2 ka BP, and this association is open to one of two possible interpretations: (1) talus accumulation was restricted to these two cold phases; or (2) talus accumulation occurred in all cold phases but earlier talus was partly buried by later talus. Thus, some old boulders were sampled and these explain the negatively-skewed frequency distribution (Fig. 5). Of these interpretations, the second is preferred because boulder lobes, active in earlier cold episodes, require sufficiently intense freeze-thaw cycles in order for frost creep and gelifluction to move them downslope (Ballantyne and Harris, 1994; van Steijn et al., 1995). Such freeze-thaw action is also likely to have caused numerous rockfalls from the cliff above the talus. However, talus may also accumulate as a consequence of paraglacial stress-release and fracture propagation in rock-slopes and/or palaeoseismicity associated with glacio-isostatic crustal uplift following local deglaciation (Ballantyne, 2002; Sass, 2006; Wilson, 2009b, in press). Therefore, it may be best to regard talus as a composite debris

accumulation of periglacial-paraglacial derivation (Wilson, 2009b). Regardless of the processes, significant talus accumulation on Muckish had effectively ceased by 7 ka BP.

If the findings reported above could be confirmed at other mountain sites in Ireland it would indicate that coarse debris landforms of these types did not finally stabilise at the end of the Younger Dryas cold period as previously implied (Quinn, 1987; Coxon, 1988). Rather, they continued to be intermittently active over the first ~4-5 ka of the Holocene, as suggested by Wilson (in press), and represent some of the geomorphological signatures of these short cold events.

6.2 Implications of the late Holocene SHD ages

Boulders of the RSF run-out debris and the debris cone yielded SHD ages from the late Holocene (Table 3, Fig. 6). The statistically indistinguishable ages from the upper and lower areas of the RSF debris are interpreted as indicating its emplacement in a single sub-cataclasmic rock-avalanche style event (sensu Jarman, 2006), rather than incremental deposition over a protracted period as characterised the accumulation of the adjacent talus. In turn this implies that the ages are close approximations to the time of failure, with a best estimate of ~1.58±1.0 ka derived from a simple average of the two ages and their confidence limits. The low-amplitude surface morphology of the run-out debris, compared with the rectilinear form of the neighbouring talus (Figs 2e-f), and the fact that the run-out debris is thin (<5 m thickness) and has over-ridden pre-existing talus is consistent with this interpretation. The slightly negatively skewed R-value frequency distributions (Fig. 5) may reflect inclusion in the samples of boulder surfaces that previously formed the cliff face and/or boulders incorporated from impact on and mixing with underlying talus. Boulders from both situations would be more weathered and of greater age than the timing of failure.

The RSF run-out debris differs considerably in its morphology, topographic position and age from those RSFs on the quartzite mountains of Donegal described by Wilson (2004), and subjected to TCND dating by Ballantyne et al. (2013), including the arcuate ridge of quarried RSF debris used here for the SHD control surfaces. These large-scale RSFs

returned ^{10}Be ages from 17.7±0.9 ka to 11.7±0.5 ka and were considered as paraglacial responses to deglaciation. The SHD age of the RSF run-out debris may indicate a millennial-scale delayed response to paraglacial stress-release, as recorded by Ballantyne et al. (2014) for a small number of RSFs in the Highlands of Scotland, or a transient triggering event whose impact was intensified because of paraglacial rockwall weakening.

A possible trigger for rock-slope failure was climatic deterioration at 2.7, 1.5 and/or 0.5 ka BP. Multiproxy palaeohydrological records from ombrotrophic bogs in the north of Ireland demonstrate rapid and major shifts to cooler and/or wetter conditions at those times (Swindles et al., 2007, 2013; Plunkett and Swindles, 2008), and are consistent with evidence for wet shifts at around the same times in mires in northern England, Scotland and parts of mainland Europe (see Swindles et al., 2007, 2013). Increases in precipitation would likely lead to a build-up of higher than normal joint-water pressures in the fractured rock of the RSF source area. Shifts to increased wetness have been proposed to explain the temporal clustering of RSFs in different parts of the European Alps at various times by Prager et al. (2008) and Borgatti and Soldati (2010), including at around 2.7 and 1.5 ka BP, and by Zerathe et al. (2014) in association with the wet shift at 4.2 ka BP. Given that the averaged SHD age and 95% confidence limit for the run-out debris overlaps with three cool and/or wet shifts (Fig. 6) the possibility that failure was triggered by excess joint-water pressure is not easily dismissed. It is interesting to note that the RSF has no apparent association with the climatic deteriorations at 5.2 and 4.2 ka BP, suggesting possible long-term progressive weakening of the rockwall as a pre-requisite for climate-triggered failure late in the Holocene.

The debris cone is envisaged as a product of high-magnitude low-frequency fluvial and debris flow events from the upland valley and from reworking of the upper part of the cone as it developed. As such the SHD ages are minimum ages for cone initiation. It is not unreasonable to infer that cone development began during or shortly after deglaciation given its extent and estimated basal thickness of ~20 m.

The SHD ages and 95% confidence limits for the debris cone overlap with one or more of the three late Holocene cool and/or wet shifts (Fig. 6). Erosive events in the

catchment probably increased in frequency and intensity during the wet shifts. Although the age from the lower part of the cone surface (~1.7±1.1 ka) indicates this area may have been stable for up to a maximum of 2.8 ka, the debris could have been emplaced as late as 0.6 ka. However, locally there is a peat cover (Fig. 2g) to 0.4 m thickness which suggests an earlier rather than later age within the 95% range.

The SHD age (0.25±0.9 ka) for boulders from the upper part of the cone encompasses the cooler/wetter period known as the Little Ice Age. This young age is consistent with the morphological 'freshness' of the debris lobes and sheets that dominate this area (Fig. 2h) and also with the whiter surface colours of the boulders compared to the grey boulders at the lower site; the implication is that the paler boulders are less weathered because they were deposited more recently. (A similar colour contrast also applies between the young and old control site boulders.). As with the early Holocene cold events, the full range of Little Ice Age geomorphological responses in the uplands of Ireland has not yet been established, but the SHD evidence from Muckish indicates that debris cone aggradation was one such impact.

The slight negative skewness of the debris cone R-value frequency distributions (Fig. 5) indicates a minor component of older boulders in the samples. These are likely to be boulders that had previous residence time in the upland valley and/or on the upper part of the cone before being transferred to the lower zone.

6.3 Comparison of SHD with TCND ages

Several studies have combined SHD and TCND in order to determine the accuracy and precision of the former method in landform dating (Sánchez et al. 2009; Winkler, 2009, 2014; Matthews and Winkler, 2011; Linge et al. in press; Tomkins et al. 2016). Although no consensus has yet been reached it has been concluded that SHD is a valuable complementary technique to TCND over a timescale that encompasses deglaciation following the LGM and the Holocene. TCND yields numerical ages for landforms and provides age control points for SHD calibration curves. It has been concluded that SHD could

be used in the selection of surfaces for TCND as it would enable greater objectivity with respect to decision making over choice of sample sites (Winkler, 2009). This in turn could reduce the number of TCND samples required and therefore overall project costs.

For the same early Holocene moraines in southern Norway, Matthews and Winkler (2011) found that SHD results were statistically indistinguishable from, but more precise than, TCND ages. Elsewhere in southern Norway, Linge et al. (in press) have shown that SHD and TCND results for early Holocene relict rock glaciers are also statistically indistinguishable. In northwest England, Tomkins et al. (2016) have established that TCND and SHD ages for retreat of the last ice sheet are of comparable accuracy and precision.

At Muckish, a similar direct comparison is not possible because none of the landforms assessed for SHD have been dated using TCND (except for the old control site). However, Ballantyne et al. (2013) applied TCND to a further seven RSFs (total of 21 boulders) on mountains adjacent to Muckish and on the same rock type. Individual boulders returned ages between 18.3±2.1 and 8.8±0.9 ka (external uncertainty ±2σ range). The ages of the four youngest boulders (11.9±1.2 – 8.8±0.9 ka: external uncertainty ±2σ range) overlap with the SHD results from the blockfield, boulder lobes and talus, but have a ±2σ range that is between 0 and 0.67 ka less than the four Muckish samples. In this instance, therefore, the TCND results appear to have a greater precision for landforms of the same general age. However, it is not clear whether, in a statistical sense, the TCND 2σ range is directly equivalent to the SHD 95% confidence interval. If this can be determined, then the precision associated with each technique could be better assessed.

7. Conclusions

SHD applied to an assemblage of late Quaternary periglacial and paraglacial landforms composed of coarse rock debris on Muckish Mountain, northwest Ireland, has revealed early Holocene stabilisation ages for blockfield, boulder lobes and talus, and a late Holocene age for RSF run-out debris and debris cone boulders. Age estimates for blockfield, boulder lobes and talus overlap with two or more of the five short intervals of marked cooling

that characterised the early Holocene, inferring that the debris was active at some of those times. Using 95% confidence intervals the summit blockfield stabilised and had become relict by ~8 ka BP, the boulder lobes had stabilised prior to the 8.2 ka BP event, and talus accumulation had ceased by ~7 ka BP. It had previously been implied that these types of landforms on Irish mountains had stabilised at the end of the Younger Dryas Stadial. The SHD results are the first indication that these early Holocene cold phases had a significant geomorphological impact in the uplands.

SHD results from RSF run-out debris imply emplacement in a single sub-cataclasmic rock-avalanche type event and indicate it to be considerably younger than other RSF debris accumulations on Muckish and adjacent mountains, which are attributed to paraglacial-related factors. The age overlaps with phases of climatic cooling and/or increased wetness in the late Holocene. Wet shifts have been proposed to explain temporal clusters of RSFs in other mountain areas and therefore a climate-trigger for the Muckish failure cannot be ignored.

Debris cone boulders, also of late Holocene age, accumulated through fluvial and debris flow events and are the most recent additions to the cone at their respective locations. The SHD results also overlap with shifts to cooler/wetter conditions and, again, are the first indication that mountain slopes in Ireland were impacted by these climate changes. Although the upper part of the cone remains intermittently active, the extent and thickness of the debris implies a lengthy period of aggradation.

Compared with TCND results from RSF boulders on adjacent mountains, the SHD ages are of similar but slightly lower precision, which reinforces the usefulness of SHD as a complementary approach to exposure-age dating of rock surfaces.

Acknowledgements

We thank Frances Wilson for assistance with data collection and Kilian McDaid and Anna Ratcliffe for preparing the diagrams.

References

Aa, A.R., Sjåstad, J. 2000. Schmidt hammer age evaluation of the moraine sequence in front of Bøyabreen, western Norway. *Norsk Geologisk Tidsskrift* 80, 27-32.

Aa, A.R., Sjåstad, J., Sønstegaard, E., Blikra, L.H. 2007. Chronology of Holocene rock-avalanche deposits based on Schmidt-hammer relative dating and dust stratigraphy in nearby bog deposits, Vora, inner Nordfjord, Norway. *The Holocene* 17, 955-964.

André, M-F. 1996. Rock weathering rates in arctic and subarctic environments (Abisko Mountains, Swedish Lapland). *Zeitschrift für Geomorphologie* 40, 499-517.

André, M-F. 2002. Rates of post-glacial rock weathering on glacially scoured outcrops (Abisko-Riksgränsen area, 68°N). *Geografiska Annaler* 84A, 139-150.

Aoyama, M. 2005. Rock glaciers in the northern Japanese Alps: palaeoenvironmental implications since the Late Glacial. *Journal of Quaternary Science* 20, 471-484.

Ballantyne, C.K. 1986. Protalus rampart development and the limits of former glaciers in the vicinity of Baosbheinn, Wester Ross. *Scottish Journal of Geology* 22, 13-25.

Ballantyne, C.K. 2002. Paraglacial geomorphology. *Quaternary Science Reviews* 21, 1935-2017.

Ballantyne, C.K., Harris, C. 1994. The periglaciation of Great Britain. Cambridge University Press, Cambridge.

Ballantyne, C.K., Stone, J.O. 2015. Trimlines, blockfields and the vertical extent of the last ice sheet in southern Ireland. *Boreas* 44, 277-287.

Ballantyne, C.K., McCarroll, D., Stone, J.O. 2007. The Donegal ice dome, northwest Ireland: dimensions and chronology. *Journal of Quaternary Science* 22, 773-783.

Ballantyne, C.K., Wilson, P., Schnabel, C., Xu, S. 2013. Lateglacial rock slope failures in north-west Ireland: age, causes and implications. *Journal of Quaternary Science* 28, 789-802.

Ballantyne, C.K., Sandeman, G.F., Stone, J.O., Wilson, P. 2014. Rock-slope failure following Late Pleistocene deglaciation on tectonically stable mountainous terrain. *Quaternary Science Reviews* 86, 144-157.

Boelhouwers, J., Jager, D.F., Joode, A. De. 1999. Application of relative-age dating methods to openwork debris flow deposits in the Cederberg Mountains, Western Cape, South Africa. *South African Geographical Journal* 81, 135-142.

Bond, G., Showers, W., Cheseby, M., Lotti, R., Almasi, P., deMenocal, P., Priore, P., Cullen, H., Hajdas, I., Bonani, G. 1997. A pervasive millennial-scale cycle in North Atlantic Holocene and glacial climates. *Science* 278, 1257-1266.

Borgatti, L., Soldati, M. 2010. Landslides as a geomorphological proxy for climate change: a record from the Dolomites (northern Italy). *Geomorphology* 120, 56-64.

Charlesworth, R.K. 1924. The glacial geology of north-west Ireland. *Proceedings of the Royal Irish Academy* 36B, 174-314.

Clark, J.A., McCabe, M., Schnabel, C., Clark, P.U., Freeman, S., Maden, C., Xu, S. 2009. ^{10}Be chronology of the last deglaciation of County Donegal, northwestern Ireland. *Boreas* 38, 111-118

Clark, R., Wilson, P. 2004. A rock avalanche deposits in Burtness Comb, Lake District, northwest England. *Geological Journal* 39, 419-430.

Clément, P., Landry, B., Yergeau, M. 1976. Déchaussement postglaciaire de filons de quartz dans les Appalaches québécoises (région de Sherbrooke, Canada). *Geografiska Annaler* 58A, 111-114.

Colman, S.M. 1981. Rock-weathering rates as functions of time. *Quaternary Research* 15, 250-264.

Colman, S.M., Dethier, D.P. (eds). 1986. *Rates of chemical weathering of rocks and minerals.* Academic Press, Orlando FL.

Cook-Talbot, J.D. 1999. Sorted circles, relative-age dating and palaeoenvironmental reconstruction in an alpine periglacial environment, eastern Jotunheimen, Norway: lichenometric and weathering-based approaches. *The Holocene* 1, 128-141.

Coxon, P. 1988. Remnant periglacial features on the summit of Truskmore, Counties Sligo and Leitrim, Ireland. *Zeitschrift für Geomorphologie* (Supplementband 71), 81-91.

Engel, Z. 2007. Measurement and age assignment of intact rock strength in the Krkonoše Mountains, Czech Republic. *Zeitschrift für Geomorphologie* 51 (Supplementband 1), 69-80.

Fabel, D., Ballantyne, C.K., Xu, S. 2012. Trimlines, blockfields, mountain-top erratics and the vertical dimensions of the last British-Irish Ice Sheet in NW Scotland. *Quaternary Science Reviews* 55, 91-102.

Ffoulkes, C., Harrison, S. 2014. Evaluating the Schmidt hammer as a method for distinguishing the relative age of late Holocene moraines: Svellnosbreen, Jotunheimen, Norway. *Geografiska Annaler* 96, 393-402.

Fjellanger J, Sørbel L, Linge H, Brook EJ, Raisbeck GM, Yiou F. 2006. Glacial survival of blockfields on the Varanger Peninsula, northern Norway. *Geomorphology* 82, 255-272.

Frauenfelder, R., Laustela, M., Kääb, A. 2005. Relative age dating of Alpine rockglacier surfaces. *Zeitschrift für Geomorphologie* 49, 145-166.

Ghilardi, B., O'Connell, M. 2013. Early Holocene vegetation and climate dynamics with particular reference to the 8.2 ka event: pollen and macrofossil evidence from a small lake in western Ireland. *Vegetation History and Archaeobotany* 22, 99-114.

Goehring BM, Brook EJ, Linge H, Raisbeck GM, Yiou F. 2008. Beryllium-10 exposure ages of erratic boulders in southern Norway and implications for the history of the Fennoscandian Ice Sheet. *Quaternary Science Reviews* 27, 320-336.

Hede, M.U., Rasmussen, P., Noe-Nygaard, N., Clarke, A.L., Vinebrooke, R.D., Olsen, J. 2010. Multiproxy evidence for terrestrial and aquatic ecosystem responses during the 8.2 ka cold event as recorded at Højby Sø, Denmark. *Quaternary Research* 73, 485-496.

Holmes, J.A., Tindall, J., Roberts, N., Marshall, W., Marshall, J.D., Bingham, A., Feeser, I., O'Connell, M., Atkinson, T., Jourdan, A-L., March, A., Fisher, E.H. 2016. Lake isotope

records of the 8200-year cooling event in western Ireland: comparison with model simulations. *Quaternary Science Reviews* 131, 341-349.

Jarman, D. 2006. Large rock slope failures in the Highlands of Scotland: characterisation, causes and spatial distribution. *Engineering Geology* 83, 161-182.

Juliussen H, Humlum O. 2007. Preservation of block fields beneath Pleistocene ice sheets on Sølen and Elgåhogna, central-eastern Norway. *Zeitschrift für Geomorphologie* 51 (Supplementband 2), 113-138.

Kellerer-Pirklbauer, A., Wangensteen, B., Farbrot, H., Etzelmüller, B. 2008. Relative surface age-dating of rock glacier systems near Hólar in Hjaltadalur, northern Iceland. *Journal of Quaternary Science* 23, 137-151.

Kłapyta, P. 2013. Application of Schmidt hammer relative age dating to Late Pleistocene moraines and rock glaciers in the western Tatra Mountains, Slovakia. *Catena* 111, 104-121.

Klitgaard-Kristensen, D., Sejrup, H.P., Haflidason, H., Johnsen, S., Spurk, M. 1998. A regional 8200 cal. yr BP cooling event in northwest Europe, induced by final stages of the Laurentide ice-sheet deglaciation? *Journal of Quaternary Science* 13, 165-169.

Knight, J., Burningham, H. 2011. Boulder dynamics on an Atlantic-facing rock coastline, northwest Ireland. *Marine Geology* 283, 56-65.

Linge, H., Nesje, A., Matthews, J.A., Fabel, D., Xu, S. in preparation. ^{10}Be surface exposure ages from relict talus-derived rock glacier lobes at Øyberget, upper Ottadalen, southern Norway.

Marshall, J.D., Lang, B., Crowley, S.F., Weedon, G.P., van Calsteren, P., Fisher, E.H., Holme, R., Holmes, J.A., Jones, R.T., Bedford, A., Brooks, S.J., Bloemendal, J., Kiriakoulakis, K., Ball, J.D. 2007. Terrestrial impact of abrupt changes in North Atlantic thermohaline circulation: early Holocene, UK. *Geology* 35, 639-642.

Matthews, J.A., Shakesby, R.A. 1984. The status of the 'Little Ice Age' in southern Norway: relative-age dating of Neoglacial moraines with Schmidt hammer and lichenometry. *Boreas* 13, 333-346.

Matthews, J.A., McEwen, L.J. 2013. High-precision Schmidt-hammer exposure-age dating of flood berms, Vetlestølsdalen, Alpine southern Norway: first application and some methodological issues. *Geografiska Annaler* 95A, 185-195.

Matthews, J.A., Owen, G. 2010. Schmidt hammer exposure-age dating: developing linear age-calibration curves using Holocene bedrock surface from the Jotunheimen-Jostedalsbreen regions of southern Norway. *Boreas* 39, 105-115.

Matthews, J.A., Wilson, P. 2015. Improved Schmidt-hammer exposure ages for active and relict pronival ramparts in southern Norway, and their palaeoenvironmental implications. *Geomorphology* 246, 7-21.

Matthews, J.A., Winkler, S. 2011. Schmidt-hammer exposure-age dating (SHD): application to early Holocene moraines and a reappraisal of the reliability of terrestrial cosmogenic-nuclide dating (TCND) at Austanbotnbreen, Joutunheimen, Norway. *Boreas* 40, 256-270.

Matthews, J.A., Nesje, A., Linge, H. 2013. Relict talus-foot rock glaciers at Øyberget, Upper Ottadalen, southern Norway: Schmidt hammer exposure ages and palaeoenvironmental implications. *Permafrost and Periglacial Processes* 24, 336-346.

Matthews, J.A., McEwen, L.J., Owen, G. 2015. Schmidt-hammer exposure-age dating (SHD) of snow-avalanche impact ramparts in southern Norway: approaches, results and implications for landform age, dynamics and development. *Earth Surface Processes and Landforms* 40, 1705-1718.

Matthews, J.A., Shakesby, R.A., Owen, G., Vater, A.E. 2011. Pronival rampart formation in relation to snow-avalanche activity and Schmidt-hammer exposure-age dating (SHD): three cases studies from southern Norway. *Geomorphology* 130, 280-288.

Matthews, J.A., Winkler, S., Wilson, P. 2014. Age and origin of ice-cored moraines in Jotunheimen and Breheimen, southern Norway: insights from Schmidt-hammer exposure-age dating. *Geografiska Annaler* 96, 531-548.

McCarroll, D. 1987. The Schmidt hammer in geomorphology: five sources of instrument error. British Geomorphological Research Group Technical Bulletin 36, 16-27.

McCarroll, D. 1989. Potential and limitations of the Schmidt hammer for relative –age dating: field tests on Neoglacial moraines, Joutunheimen, southern Norway. *Arctic and Alpine Research* 21, 268-275.

McCarroll, D. 1994. The Schmidt hammer as a measure of the degree of rock surface weathering and terrain age. In: Beck, C. (ed.), Dating in exposed and surface contexts. University of New Mexico Press, Albuquerque, 29-46.

McEwan, L., Matthews, J.A. 2013. Sensitivity, persistence and resolution of the geomorphological record of valley-floor floods in an alpine glacier-fed catchment, Leirdalen, Jotunheimen, southern Norway. *The Holocene* 23, 974-989.

McEwan, L., Matthews, J.A., Owen, G., Shakesby, R.A. In prep. Paraglacial development and late-Holocene stability of the Illåi alluvial fan, Jotunheimen, Norway.

Nesje, A., Blikra, L.H., Anda, E. 1994. Dating rockfall-avalanche deposits from degree of rock-surface weathering by Schmidt-hammer tests: a study from Norangsdalen, Sunnmøre, Norway. *Norsk Geologisk Tidsskrift* 74, 108-113.

Nicholson, D. 2008. Rock control on microweathering of bedrock surface in a periglacial environment. *Geomorphology* 101, 655-665.

O'Cofaigh, C., Dunlop, P., Benetti, S. 2012. Marine geophysical evidence for Late Pleistocene ice sheet extent and recession off northwest Ireland. *Quaternary Science Reviews* 44, 147-159.

Owen, G., Matthews, J.A., Albert, P.G. 2007. Rates of Holocene chemical weathering, 'Little Ice Age' glacial erosion and implications for Schmidt-hammer dating at a glacier-foreland boundary, Fåbergstølsbreen, southern Norway. *The Holocene* 17, 829-834.

Owen, G., Hiemstra, J.F., Matthews, J.A., McEwen, L.J. 2010. Landslide-glacier interaction in a neoparaglacial setting at Tverrbytnede, Joutunheimen, southern Norway. *Geografiska Annaler* 92A, 421-436.

Plunkett, G., Swindles, G.T. 2008. Determining the Sun's influence on Lateglacial and Holocene climates: a focus on climate response to centennial-scale solar forcing at 2800 cal. BP. *Quaternary Science Reviews* 27, 175-184.

Prager, C., Zangerl, C., Patzelt, G., Brander, R. 2008. Age distribution of fossil landslides in the Tyrol (Austria) and its surrounding areas. *Natural Hazards Earth System Science* 8, 377-407.

Proceq, 2006. Operating instructions (Betonprüfhammer N/NR-L/LR). Proceq SA, Schwerzenbach.

Quinn, I.M. 1987. The significance of periglacial features on Knocknadobar, south west Ireland. In: Boardman J (ed.), Periglacial processes and landforms in Britain and Ireland. Cambridge University Press, Cambridge, 287-294.

Rode, M., Kellerer-Pirklbauer, A. 2012. Schmidt-hammer exposure-age dating (SHD) of rock glaciers in the Schöderkogel-Eisenhut area, Schladminger Tauern Range, Austria. *The Holocene* 22, 761-771.

Rohan, P.K. 1986. *The climate of Ireland*. Stationery Office, Dublin.

Rundberg, S. 1970. Naturgeografiska seminarieuppsatser vid Göteborgs universitet höstterminen 1959-vårterminen 1969. *Meddelanden från Geografiska Föreningen i Göteborg, Gothia* 10, 1-172.

Sánchez, J.S., Mosquera, D.F., Romaní, J.R.V. 2009. Assessing the age-weathering correspondence of cosmogenic ^{21}Ne dated Pleistocene surface by the Schmidt Hammer. *Earth Surface Processes and Landforms* 34, 1121-1125.

Sass, O. 2006. Determination of the internal structure of alpine talus deposits using different geophysical methods (Lechtaler Alps, Austria). *Geomorphology* 80, 45-58.

Sellier, D., Wilson, P. 1995. Muckish – alluvial cone. In: Wilson, P. (ed.) *North-west Donegal: Field Guide No. 19.* Irish Association for Quaternary Studies, Dublin, 53-54.

Shakesby, R.A., Matthews, J.A., Owen, G. 2006. The Schmidt hammer as a relative-age dating tool and its potential for calibrated-age dating in Holocene glaciated environments. *Quaternary Science Reviews* 25, 2846-2867.

Shakesby, R.A., Matthews, J.A., Karlén, W., Los, S.O. 2011. The Schmidt hammer as a Holocene calibrated-age dating technique: testing the form of the R-value-age relationship and defining the predicted age errors. *The Holocene* 21, 615-628.

Sjöberg, R., 1990. Measurement and calibration of weathering processes and lichenometric investigations on a wave washed moraine, Bådamalen, on the upper Norrland coast, Sweden. *Geografiska Annaler* 72A, 319-327.

Sjöberg, R., Broadbent, N. 1991. Measurement and calibration of weathering, using the Schmidt hammer, on wave washed moraines on the upper Norrland coast, Sweden. *Earth Surface Processes and Landforms* 16, 57-64.

Snowball, I., Muscheler, R., Zillén, L., Sandgren, P., Stanton, T., Ljung, K. 2010. Radiocarbon wiggle matching of Swedish lake varves reveals asynchronous climate changes around the 8.2 kyr cold event. *Boreas* 39, 720-733.

Stahl, T., Winkler, S., Quigley, M., Bebbington, M., Duffy, B., Duke, D. 2013. Schmidt hammer exposure-age dating (SHD) of late Quaternary fluvial terraces in New Zealand. *Earth Surface Processes and Landforms* 38, 1838-1850.

Stephenson, W.J., Kirk, R.M. 2000. Development of shore platforms on Kaikoura Peninsula, South Island, New Zealand II: the role of subaerial weathering. *Geomorphology* 32, 43-56.

Swindles, G.T., Plunkett, G., Roe, H.M. 2007. A multiproxy climate record from a raised bog in County Fermanagh, Northern Ireland: a critical examination of the link between bog surface wetness and solar variability. *Journal of Quaternary Science* 22, 667-679.

Swindles, G.T., Lawson, I.T., Matthews, I.P., Blaauw, M., Daley, T.J., Charman, D.J., Roland, T.P., Plunkett, G., Schettler, G., Gearey, B.R., Turner, T.E., Rea, H.A., Roe, H.M., Amesbury, M.J., Chambers, F.M., Holmes, J., Mitchell, F.J., Blackford, J., Blundell, A., Branch, N., Holmes, J., Langdon., P., McCarroll, J., McDermott, F., Oksanen, P.O., Pritchard, O., Stastney, P., Stefanini, B., Young, D., Wheeler, J., Becker, K., Armit, I. 2013. Centennial-scale climate change in Ireland during the Holocene. *Earth-Science Reviews* 126, 300-320.

Tomkins, M.D., Dortch, J.M., Hughes, P.D. 2016. Schmidt Hammer exposure dating (SHED): Establishment and implications for the retreat of the last British Ice Sheet. *Quaternary Geochronology* 33, 46-60.

van Steijn, H., Bertran, P., Francou, B., Hétu, B., Texier, J-P. 1995. Models for the genetic and environmental interpretation of stratified slope deposits: review. *Permafrost and Periglacial Processes* 6, 125-146.

Vincent, P.J., Lord, T.C., Telfer, M.W., Wilson, P. 2011. Early Holocene loessic colluviation in northwest England: new evidence for the 8.2 ka event in the terrestrial record? *Boreas* 40, 105-115.

Vinther, B.M., Clausen, H.B., Johnsen, S.J., Rasmussen, S.O., Andersen, K.K., Buchardt, S.L., Dahl-Jensen, D., Seierstad, I.K., Siggaard-Andersen, M-L., Steffensen, J.P., Svensson, A., Olsen, J., Heinemeier, J. 2006. A synchronized dating of three Greenland ice cores throughout the Holocene. *Journal of Geophysical Research* 111, D13102.

White, K., Bryant, R., Drake, N. 1998. Techniques for measuring rock weathering: application to a dated fan segment sequence in southern Tunisia. *Earth Surface Processes and Landforms* 23, 1031-1043.

Wicks, K., Mithen, S. 2014. The impact of the abrupt 8.2 ka cold event on the Mesolithic population of western Scotland: a Bayesian chronological analysis using 'activity events' as a population proxy. *Journal of Archaeological Science* 45, 240-269.

Wilson, P. 1990a. Morphology, sedimentological characteristics and origin of a fossil rock glacier on Muckish Mountain, northwest Ireland. *Geografiska Annaler* 72A, 237-247.

Wilson, P. 1990b. Clast size variations on talus: some observations from northwest Ireland. *Earth Surface Processes and Landforms* 15, 183-188.

Wilson, P. 1993. Description and origin of some talus-foot debris accumulations, Aghla Mountains, Co, Donegal, Ireland. *Permafrost and Periglacial Processes* 4, 231-244.

Wilson, P. 2004. Relict rock glaciers, slope failure deposits, or polygenetic features? A re-assessment of some Donegal debris landforms. *Irish Geography* 37, 77-87.

Wilson, P. 2007. The Kirkby Fell rock-slope failure, Malham, Yorkshire Dales. *North West Geography* 7, 1-9.

Wilson, P. 2009a. Storurdi: a late Holocene rock-slope failure (sturzstrom) in the Jotunheimen, southern Norway. *Geografiska Annaler* 91A, 47-58.

Wilson, P. 2009b. Rockfall talus slopes and associated talus-foot features in the glaciated uplands of Great Britain and Ireland: periglacial, paraglacial or composite landforms? In: Knight, J., Harrison, S. (eds), Periglacial and paraglacial processes and environments. The Geological Society, London, Special Publication 320, 133-144.

Wilson, P. in press. Periglacial and paraglacial processes, landforms and sediments. In: Coxon, P., McCarron, S. (eds), Advances in Quaternary Science: The Irish Quaternary. Springer.

Wilson, P., Sellier, D. 1995. Active patterned ground and cryoturbation on Muckish Mountain, Co. Donegal, Ireland. *Permafrost and Periglacial Processes* 6, 15-25.

Wilson, P., Matthews, J.A., Mourne, R.W. 2016. Relict blockstreams at Insteheia, Valldalen-Tafjorden, southern Norway: their nature and Schmidt-hammer exposure age. *Permafrost and Periglacial Processes*

Winkler, S. 2005. The Schmidt hammer as a relative-age dating technique: potential and limitations of its application on Holocene moraines in Mt Cook National Park, Southern Alps, New Zealand. *New Zealand Journal of Geology and Geophysics* 48, 105-116.

Winkler, S. 2009. First attempt to combine terrestrial cosmogenic nuclide (10Be0 and Schmidt hammer relative-age dating: Strauchon Glacier, Southern Alps, New Zealand. *Central European Journal of Geosciences* 1, 274-290.

Winkler, S. 2014. Investigation of late-Holocene moraines in the western Southern Alps, New Zealand, applying Schmidt-hammer exposure-age dating. *The Holocene* 24, 48-66.

Winkler, S., Matthews, J.A. 2014. Comparison of electronic and mechanical Schmidt hammers in the context of exposure-age dating: are *Q*- and *R*-values interconvertible? *Earth Surface Processes and Landforms* 39, 1128-1136.

Winkler, S., Matthews, J.A., Mourne, R.W., Wilson, P. 2016. Schmidt-hammer exposure ages from periglacial patterned ground in Jotunheimen, Norway, and their interpretive problems. *Geografiska Annaler*

Zerathe, S., Lebourg, T., Braucher, R., Bourlès, D. 2014. Mid-Holocene cluster of large-scale landslides revealed in the southwestern Alps by ^{36}Cl dating. Insight on an Alpine scale landslide activity. *Quaternary Science Reviews* 90, 106-127.

Zillén, L., Snowball, I. 2009. Complexity of the 8 ka climate event in Sweden recorded by varved lake sediments. *Boreas* 38, 493-503.

Figure captions:

Fig. 1. Muckish Mountain, northwest Ireland, showing locations of the periglacial and paraglacial landforms selected for SHD.

Fig. 2. Views of the debris landforms on Muckish at which SHD was conducted. (**a**) The quarried debris of the RSF deposit (middle distance). The location of the young control site, within the quarried debris, is indicated by the red marker lower left; the old control site, on the flanks of the debris ridge, is indicated by the red marker upper right. (**b**) Surface boulders at the old control site on proximal slope of the RSF deposit. (**c**) Summit blockfield sampling location. (**d**) Boulder lobe at the upper sampling location on the west-facing slopes of Muckish. (**e**) Part of the talus slope above the RSF shown in photo a; SHD was conducted on boulders near the base of the talus. (**f**) RSF run-out debris adjacent to the talus shown in photo e; the red markers indicate the upper and lower sampling locations. (**g**) Debris cone adjacent to the RSF shown in photo f; the red markers indicate the upper and lower sampling locations. (**h**) Upper sampling location at the apex of the debris cone shown in photo g.

Fig. 3. Frequency distributions of Schmidt-hammer R-values for the young and old control sites. N=150 and the class interval is 2 units.

Fig. 4. High-precision calibration curve and equation based on Schmidt-hammer data for young and old control sites.

Fig. 5. Frequency distributions of Schmidt-hammer R-values for the debris landforms. N=150 and the class interval is 2 units.

Fig. 6. Plot of NGRIP ice-core δO^{18} data (from Vinther et al., 2006), intervals of well documented Holocene climatic deterioration in the northeast Atlantic region (vertical grey bands – cold events in early Holocene, cool and/or wet events in mid and late Holocene) from Bond et al. (1997) and Vinther et al. (2006), and SHD ages with 95% confidence limits for the coarse debris landforms on Muckish. Landform codes are given on Figure 1; u: upper site, l: lower site.

Tables:

Table 1. Schmidt-hammer R-values and associated statistics for the control sites. Mean R-values are based on the means of two impacts on each of 150 boulders; confidence intervals use n=150 boulders.

Table 2. Schmidt-hammer R-values and associated statistics for the sampled landforms. Mean R-values are based on the means of two impacts on each of 150 boulders; confidence intervals use n=150 boulders.

Table 3. Schmidt-hammer exposure-ages for the sampled landforms. Each SHD age has a 95% confidence interval (C_t) derived from the sampling error of the landform sample (C_s) and the error associated with the calibration curve (C_c).

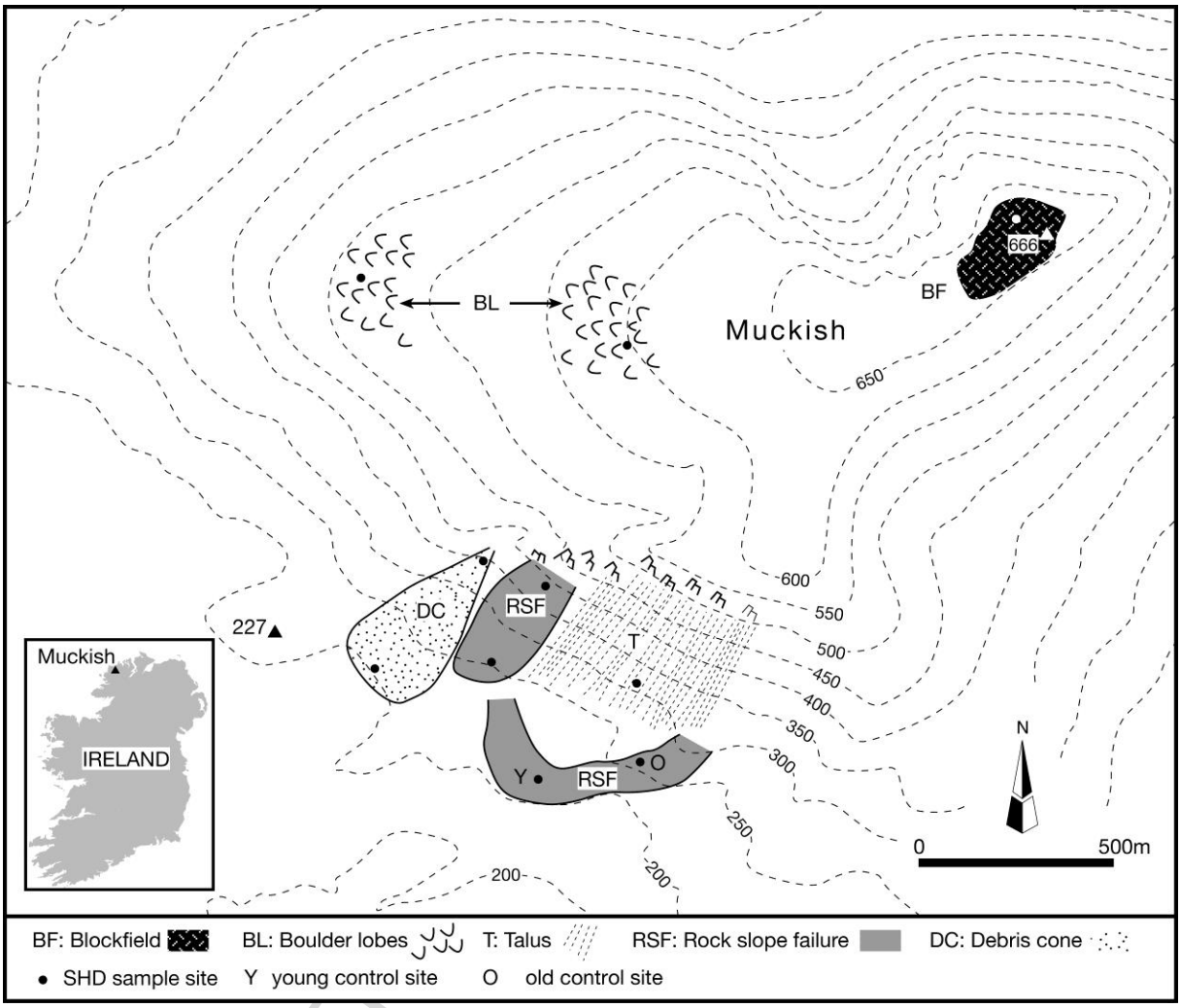

Fig. 1

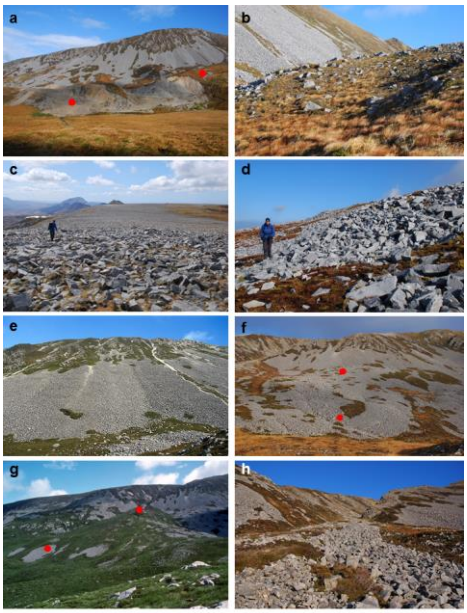

Fig. 2

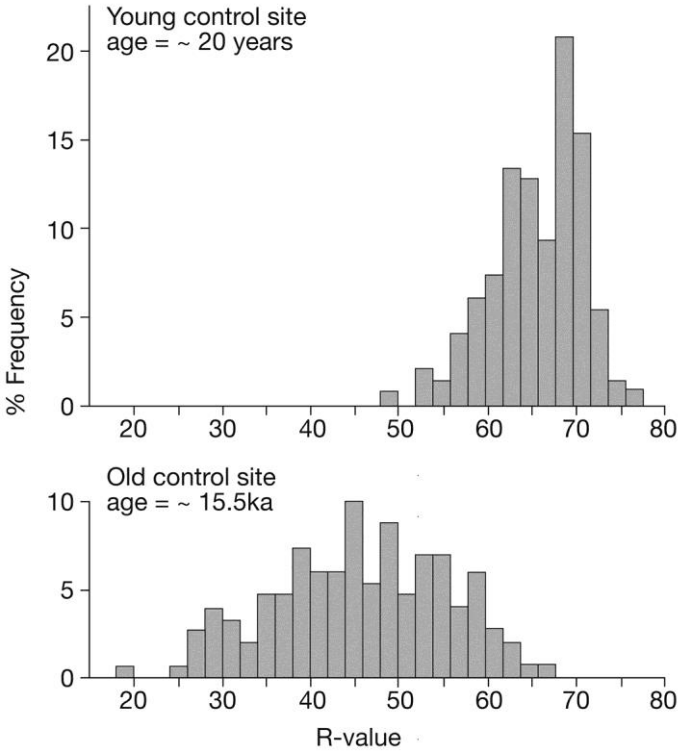

Fig. 3

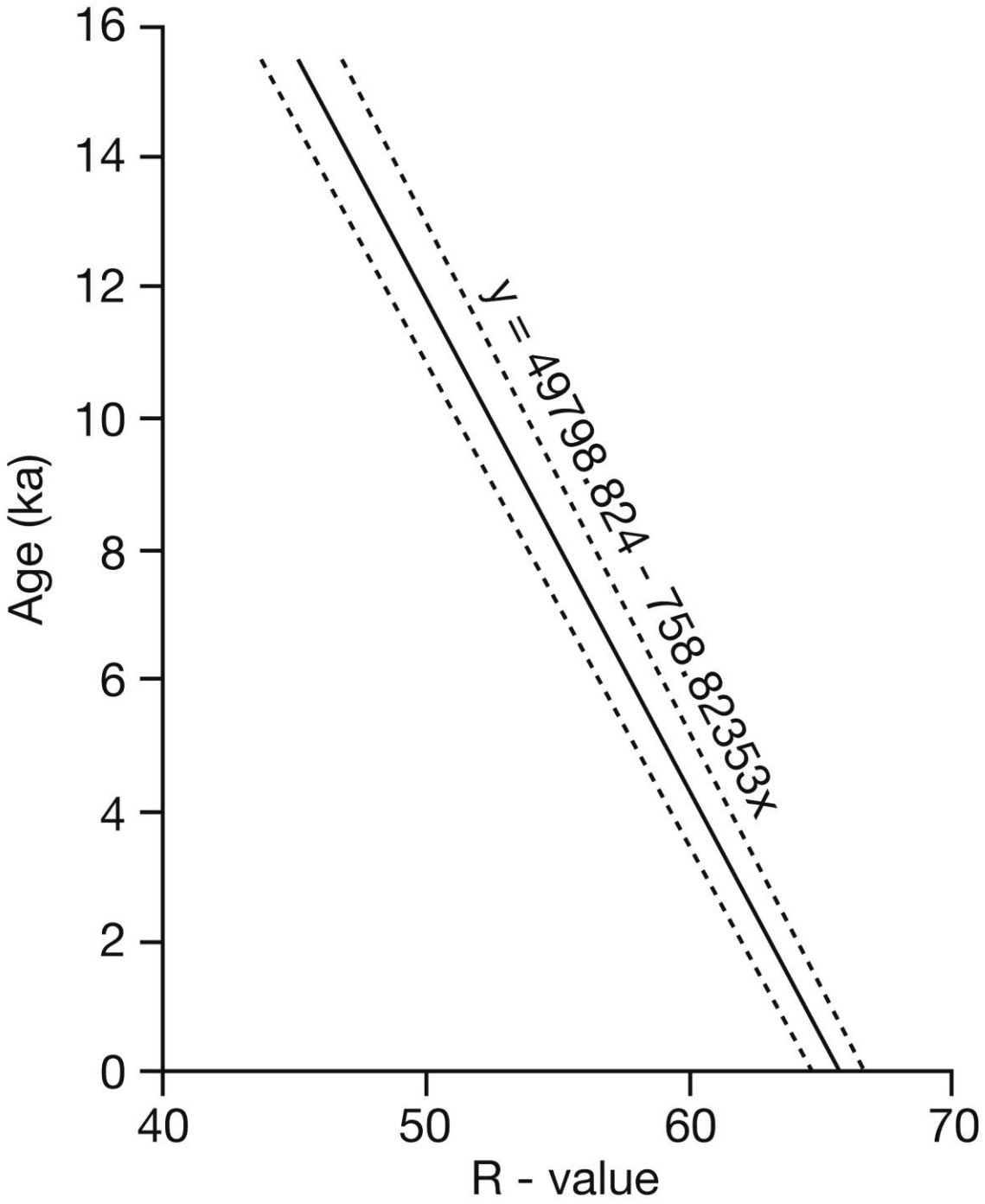
16
14
12
10
8
6
4
2
0
Age (ka)
40
50
60
70
R - value
y = 49798.824 - 758.82353x

Fig. 4

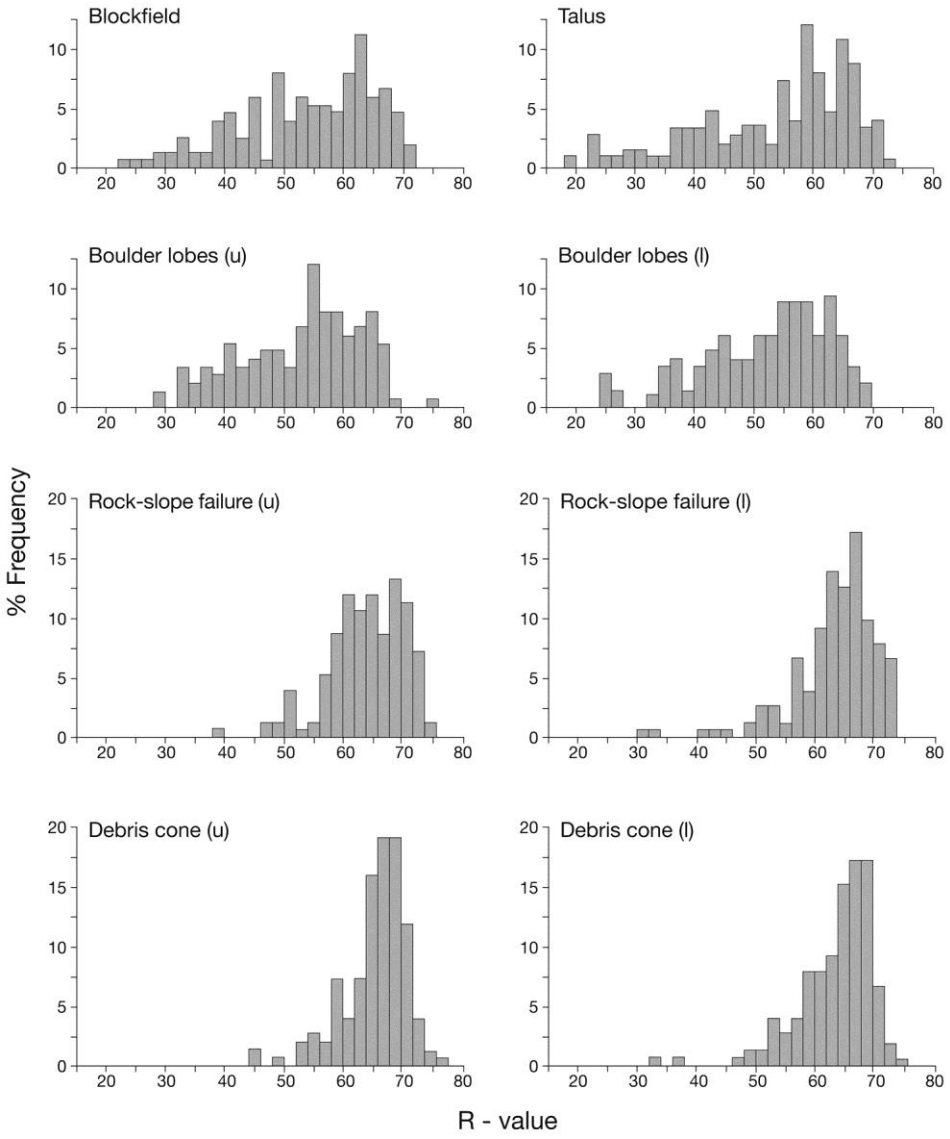
Blockfield
Talus
Boulder lobes (u)
Boulder lobes (l)
Rock-slope failure (u)
Rock-slope failure (l)
Debris cone (u)
Debris cone (l)
% Frequency
R - value

Fig. 5

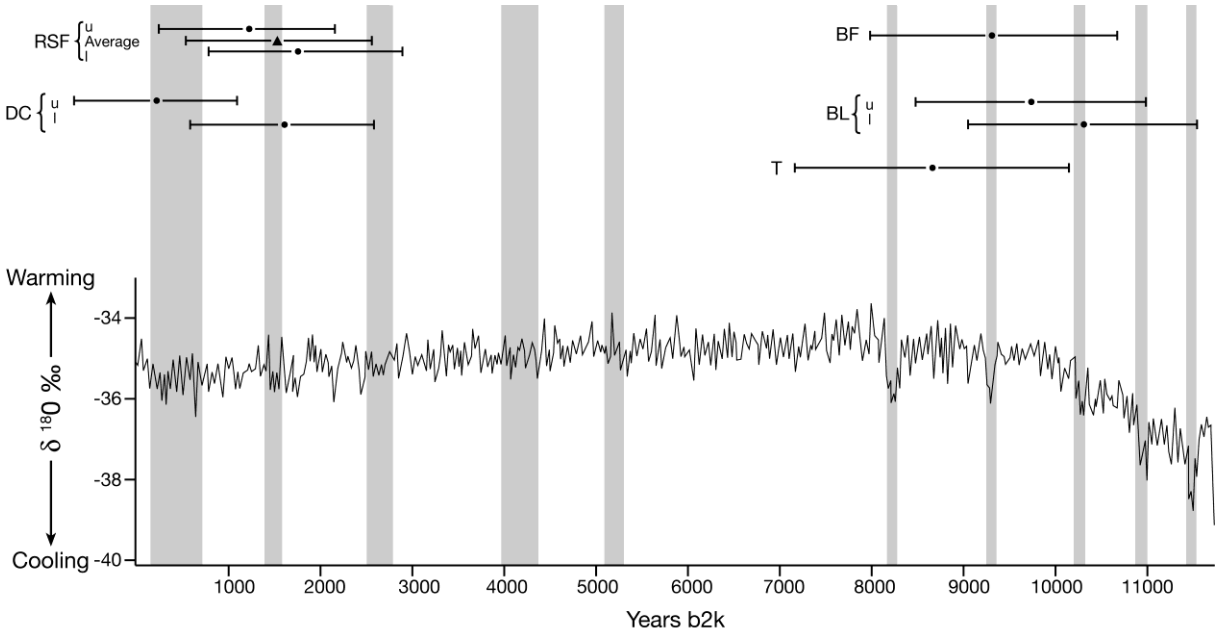

Fig. 6

Table 1. Schmidt-hammer R-values for the control sites.

Control site	Age (years)	Mean R-value (n=150)	Standard deviation	Standard error	Confidence interval (95%)
Young	~20	65.6	5.17	0.42	0.83
Old	~15,500	45.2	9.92	0.81	1.60

Table 2. Schmidt-hammer R-values for the sampled landforms.

Sample	Mean R-value	Standard	Standard	Confidence
	(n=150)	deviation	error	interval (95%)
Blockfield	53.4	11.36	0.93	1.83
Boulder lobes (u)	52.8	9.95	0.82	1.62
Boulder lobes (l)	52.1	10.53	0.86	1.70
Talus	54.2	12.53	1.03	2.04
Rock-slope failure (u)	63.9	6.54	0.54	1.06
Rock-slope failure (l)	63.2	7.28	0.60	1.18
Debris cone (u)	65.3	5.52	0.45	0.89
Debris cone (l)	64.3	6.51	0.53	1.05

u: upper site
l: lower site

Table 3. Schmidt-hammer exposure-ages (SHD) for the sampled landform. Each SHD age has a 95% confidence interval (Ct) derived from the sampling error of the landform sample (Cs) and the error associated with the calibration curve (Cc).

Landform	SHD age	*Ct*	*Cs*	*Cc*
	(years)	(years)	(years)	(years)
Blockfield	9278	±1408	1388.7	234.9
Boulder lobes (u)	9733	±1248	1229.3	217.7
Boulder lobes (l)	10,264	±1305	1290	197.6
Talus	8671	±1569	1548	257.8
Rock-slope failure (u)	1310	±966	804.4	535.6
Rock-slope failure (l)	1841	±1033	895.4	515.6
Debris cone (u)	248	±929	675.4	638.4
Debris cone (l)	1689	±1056	796.8	692.8

u: upper site
l: lower site